ACADEMIC PRESS

Available online at www.sciencedirect.com

SCIENCE DIRECT®

Journal of Sound and Vibration 262 (2003) 1191–1222

JOURNAL OF SOUND AND VIBRATION

www.elsevier.com/locate/jsvi

Parametric-resonance-induced cable vibrations in network cable-stayed bridges. A continuum approach

G.F. Royer-Carfagni*

Department of Civil–Environmental Engineering and Architecture, University of Parma, Parco Area delle Scienza 181/A, I43100 Parma, Italy

Received 1 August 2001; accepted 30 May 2002

Abstract

There is a wealth of evidence to suggest that the bearing cables of cable-stayed bridges may experience large-amplitude oscillations, attributed in general to parametric resonance with the girder vibrations. A common coutermeasure consists of connecting the principal stays together with secondary cables to form a network and, here, optimal cable arrangments will be discussed when such a network is uniform and triangular meshed. The present approach is qualitative, and basically consists of homogenizing the cable net to an orthotropic elastic membrane, and then considering an auxiliary structure where the bridge girder, instead of being supported by the cable network, is supported by wedge-shaped membranes. The elastic solution under uniformly distributed loads, found using Lekhnitskii's approach, is the starting point for the discussion of the system in dynamic equilibrium. Having established a correspondence between the cable-net size and shape and the elastic moduli of the homogenized membrane, simple formulas are obtained to describe the *global* bridge vibration, as well as the *local* oscillations of the cables. It is then possible to estimate the girder and cable-net characteristic frequencies, to evaluate those conditions possibly leading to parametric resonance and, with respect to these variables, to determine optimal cable arrangements. This method is finally applied to the paradigmatic example of the Normandy Bridge.

1. Introduction

Consideration of recent problems provides evidence that the bearing stays of cable-stayed bridges can undergo large amplitude vibrations [1]. For example, important oscillations were observed in the stays of the Brotonne Bridge [2] just after its opening and, despite the fact that the girder oscillations were hardly perceptible, the dynamic cable sag was of the order of meters.

*Tel.: +39-0521-905917; fax: +39-0521-905924.
E-mail address: gianni.royer@unipr.it (G.F. Royer-Carfagni).

0022-460X/03/$ - see front matter
doi:10.1016/S0022-460X(02)01149-5

To shore them up, truck dampers were placed at the base of the stays, but the precariousness and, somehow, the brutality of the adopted countermeasure, testifies to how unexpectedly the problem occurred. The phenomenon has been observed by long-term monitoring of other modern cable-stayed bridges, as in the case of the Annancis [3], Faro [4], Tjörn [5], Tampico [6], Helgeland [7], Ben-Ahin and Wandre [8] bridges, to mention just a few examples in Europe.

Although there is no universal agreement about the causes of vibration, possible explanations essentially follow two different ways of thinking. According to the first rationale, vibrations are due to external environmental actions acting directly on the stays. In particular, the wind-tunnel experiments by Hikami and Shiraishi [9] have shown that it is the combination of rain and wind, rather than their separate action, that provokes aerodynamic instability. The excitation is due to the change in shape of the stay-sheath profile, produced by the wind-induced formation of a water rill at the extrados of the cable. A completely different explanation points instead to an interaction between the vibrations of the stays and the oscillations of their extremities anchored to girder and pylons [10]. If some resonance conditions are satisfied, energy can flow to the stays and provoke their large-amplitude oscillations. Each of these aspects has been the subject of careful investigations [11], in many cases followed by laboratory and in situ testing [12].

In this paper, only this second type of instability will be explicitly considered, but some of the deductions that follow might also be applied to the rain–wind-induced vibrations. In particular, the discussion will focus on the advantages of a countermeasure commonly adopted in the design practice, which consists of linking the stays together with secondary inter-ties, sometimes referred to as counter-stays, to form a cable network. Many important bridges, likewise Leonhardt's proposal for the Messina strait crossing [13] or the Normandy bridge [14–16], make use of such a system of secondary cables, connecting intermediate points of the main stays to the girder.

To illustrate this, reference will be made to the classical layout of a three-span bridge, of the type represented in Fig. 1. Here, the girder is attached to pylons by a triangular-mesh net, formed by three orders of parallel elastic cables firmly connected at the intersection points. This scheme derives from a traditional cable-stayed bridge of the harp type whose stays, referred to as the *principal stays* (emphasized in bold lines in Fig. 1), are connected by two sets of parallel wires, referred to as the *secondary cables*, inclined at a fixed angle with respect to the principal stays.

In order to treat the problem in analytical form, the following hypotheses are introduced: (i) the secondary stays have been properly pre-tensioned, so that they can withstand limited compressive loads as tension decreases; (ii) the cables are small in diameter and very numerous; (iii) the principal stays, as well as the secondary cables, respectively, have a constant cross-section,

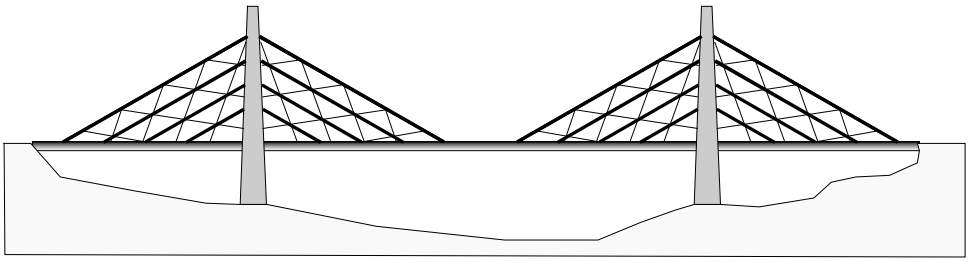

Fig. 1. Typical network cable-stayed-bridge layout.

and are equidistant; (iv) the bridge girder is axially stiff and perfectly flexible in bending, while the pylons are rigid.

Hypothesis (i) reflects the common practice in most cable-stayed bridges with counter-stays (see for example Ref. [13] or [15]). In fact, for safety and durability requirements, the counter-stays are pre-tensioned to avoid their slackening under live loads. Condition (ii) is almost a rule in modern design: for many reasons, first of all maintenance feasibility (i.e., stay replacement), it is preferable to have many small-diameter stays rather than just a few large-diameter cables [17]. Postulating a continuous 'curtain' will provide the basis for an analytical approach to the problem.

Hypotheses (iii) and (iv) may appear less realistic, since in most bridges the stay cross-sections are usually not constant, deck flexural inertia is not negligible and pylon deformation may be considerable. However, there are at least two cases in which such conditions are acceptable: medium-span slender-deck bridges and long-span bridges.

During the last decade, the new design "concept" of slender-deck cable-stayed bridges has proved to be both economical and aesthetically pleasing for medium-span bridges (around 200 m) [17]. From a static point of view, a slender deck is useful for reducing the bending moment under live loads, but slenderness enhances bridge deflection. This, however, is not an insurmountable problem, since the bridge sag under dead loads can be compensated by a properly designed camber, while the sag under live loads can be limited by strengthening the bridge pylons (either increasing their inertia, or connecting the back stays to massive anchorage blocks). In medium-span bridges, the deck is usually reduced to a simple concrete slab (30–50 cm thick), with considerable advantages for both construction and long-term durability (the Diepolsau bridge in Switzerland [17] is a paradigmatic example). In bridges of this kind, a large deck cross-sectional area is associated with a negligible flexural inertia, as well as stiff pylons. Moreover, the heaviness of the concrete deck results in dead loads that usually exceed live loads. Since dead loads are uniformly distributed, in bridges of the harp-type the principal-stay cross-sections are practically constant.

Similar considerations also hold true for long-span cable-stayed bridges. Now, structural feasibility, aeroelastic stability, serviceability and—why not—aesthetics, force the limitation of the girder-beam height to a small fraction of the main span of the bridge. For long-span cable-stayed bridges, which meet the aforementioned characteristics of medium-span slender-deck bridges, hypotheses (iii) and (iv) may thus be considered, albeit approximately, verified.

These assumptions will allow the conception, through homogenization of the cable-net, of an ideal model in linear elasticity to study the structural scheme of Fig. 1. The continuum approach will provide simple formulas for the rapid calculation of the most important dynamic parameters, to be used in the preliminary design phases. Of course, this method does not intend and cannot replace an FEM analysis, which should always corroborate the final design. Nevertheless, a closed-form solution, though approximate, may be helpful to the designer, since it allows a comprehensive and concise view of the role played by the various parameters, in particular by the cable-net shape and size.

The outline of the present paper is the following. In Section 2, germane to the analysis of the continuum model, the phenomenon of parametric resonance is introduced for the case of one vibrating stay. In Section 3, a correspondence is established, through homogenization, between a real bridge and an ideal boundary value problem in linear elasticity, i.e., that of a uniformly loaded flexible beam suspended by an anisotropic elastic wedge-shaped membrane. For this elastic model a closed-form solution is calculated, which will be used in Section 4 for determining the

system's natural frequencies. In Section 5, the dynamic behavior of the model is further investigated in response to pulsing loads acting on the girder, with emphasis on possible parametric resonance conditions. Because of the established correlation between the elastic moduli of the membrane and the shape and size of the cable network, it will be possible to investigate optimal cable-net arrangements to contain stay oscillations in a real bridge. Finally, in Section 6, the continuum approach will be applied to the representative example of the Normandy Bridge.

2. Preliminaries. Parametric resonance for one vibrating stay

Parametric resonance instability occurs when one of the parameters that influence the system natural vibrations varies with time due to the action of external causes. This phenomenon has been mentioned by Kovàcs [10] to explain the large amplitude oscillations of the stays, in which it is the variation of their axial stress due to girder movements that provokes the instability. Kovàcs considers one stay isolated from the remaining structure and, neglecting the cable slope, examines a problem similar to that of Fig. 2. Here, a vertical linear-elastic string, of length L, cross-sectional area A, mass-per-unit-length ρ and Young's modulus E, is suspended at the upper extremity, while it supports a mass M, representative of the deck, and its lower end. Since $M \gg \rho L$, in static equilibrium the cable is vertical and its axial force N_0 is approximately constant and equal to Mg (g is the gravity acceleration). Kovàcs models the effect of the anchor-point movements as an equivalent pulsing vertical load $P = P_0 \sin(2\Omega t)$, applied at the cable lower extremity as in Fig. 2. Such movements are due to the girder oscillations, caused in general by environmental or traffic loads.

Despite the resulting model being very well known [18], it is now recalled in detail because the classical hypotheses used in the one-dimensional case will be naturally extended to two dimensions (2-D). With reference to the system (x, y) of Fig. 2, let $u = u(x, t)$ and $v = v(x, t)$ represent the displacement components in the x and y directions for particles initially at x for $t = 0$. The partial derivative of $u(x, t)$ with respect to x and t, respectively, will be denoted by $u_{,x}$ and $u_{,t}$. Then, the crucial hypothesis, due to Kirchhoff [19], consists in assuming that when the string moves from the vertical reference equilibrium configuration, its axial strain is approximated by

$$\varepsilon = u_{,x} + \tfrac{1}{2} v_{,x}^2, \tag{1}$$

so that strain energy reads

$$U = N_0 \int_0^L \left(u_{,x} + \tfrac{1}{2} v_{,x}^2\right) \mathrm{d}x + \tfrac{1}{2} EA \int_0^L \left(u_{,x} + \tfrac{1}{2} v_{,x}^2\right)^2 \mathrm{d}x. \tag{2}$$

Thus, assuming still under Kirchhoff [19] that $u_{,t}(x, t) \ll v_{,t}(x, t)$ in the kinetic energy, a standard application of Hamilton's principle with the boundary conditions

$$\begin{aligned} u(0, t) &= 0, \\ v(0, t) &= 0, \\ v(L, t) &= 0 \end{aligned} \tag{3}$$

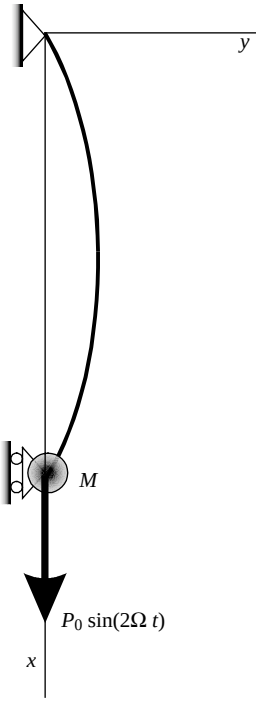

Fig. 2. The vibrating stay model.

gives the field equations

$$EA\frac{\partial}{\partial x}(u_{,x}+\tfrac{1}{2}v_{,x}^2)=0 \tag{4}$$

$$-\rho v_{,tt}+N_0 v_{,xx}+EA\frac{\partial}{\partial x}\left[v_{,x}\left(u_{,x}+\tfrac{1}{2}v_{,x}^2\right)\right]=0 \tag{5}$$

and the natural condition

$$EA[u_{,x}(L,t)+\tfrac{1}{2}(v_{,x}(L,t))^2]=P_0\sin(2\Omega t). \tag{6}$$

From Eq. (4), it is easily seen that $EA(u_{,x}+\frac{1}{2}v_{,x}^2)$ is a function of t only and, from Eq. (6), this equals $P_0\sin(2\Omega t)$. Thus, eliminating $u(x,t)$ in the resulting system of equations, the problem is governed by

$$-\rho v_{,tt}+[N_0+P_0\sin(2\Omega t)]v_{,xx}=0 \tag{7}$$

to which the boundary conditions $(3)_2$ and $(3)_3$ must be added.

To solve Eq. (7), the solutions are expanded in uniformly convergent sequences in the form $v(x,t)=\sum_{k=1}^{\infty} w_k(x)\,q(t)$. Inserting the resulting expressions into Eq. (7) and requiring that all of

the terms of the sequence are zero, one obtains the eigenvalue problem

$$w_k'' + \zeta_k w_k = 0,$$
$$\rho \ddot{q}_k + \zeta_k [N_0 + P_0 \sin(2\Omega t)] q_k = 0. \tag{8}$$

From the first of these equations, taking into account Eqs. $(3)_2$ and $(3)_3$, it is immediately found that $\zeta_k > 0$ and $w_k = C_k \sin(k\pi x/L)$, which represents the kth modal shape. The corresponding kth eigenvalue takes the form

$$\zeta_k = \frac{k^2\pi^2}{L^2},$$

so that Eq. $(8)_2$ reduces to

$$\ddot{q}_k + \frac{k^2\pi^2}{\rho L^2}[N_0 + P_0 \sin(2\Omega t)] q_k = 0.$$

Let now ω_k denote the quantity

$$\omega_k = \sqrt{\frac{k^2\pi^2 N_0}{\rho L^2}}, \tag{9}$$

which represents the natural frequency of the string now supposed fixed at its extremities. Introducing the normalized variable $\tau = (\Omega t - \pi)$, one obtains the canonical expression for Mathieu's equation

$$\frac{\mathrm{d}^2}{\mathrm{d}\tau^2} q_k + [\lambda_k - 2\mu_k \sin(2\tau)] q_k = 0, \tag{10}$$

where the parameters λ_k and μ_k are given by

$$\lambda_k = \frac{\omega_k^2}{\Omega^2}, \quad \mu_k = \frac{\omega_k^2}{\Omega^2}\frac{P_0}{2N_0}. \tag{11}$$

Since Eq. (10) is a linear differential equation with real periodic coefficients, the general theory by Floquet assures that it supports solutions unlimited in time depending upon the values of the coefficients λ_k and μ_k [18]. The corresponding instability conditions are summarized in stability charts of the type represented in Fig. 3, where the instable regions in the plane (λ, μ) are hatched in the picture. From Eq. (11), notice that, for fixed N_0 and P_0, the points of interest in the (λ, μ) plane lie on the lines

$$\lambda_k = \frac{2N_0}{P_0}\mu_k. \tag{12}$$

Now, condition $N_0 \gg P_0$ is certainly verified for a vibrating bridge-stay. This means that the lines (12) are almost vertical (dotted line in Fig. 3). It thus follows from Fig. 3 that the system oscillations become unbounded when λ_k is in a neighborhood of the values 1, 4, 9 and so on. The first instability condition occurs when $\lambda_k \simeq 1$, corresponding to the case in which $\omega_k \simeq \Omega$, i.e., the frequency of the external load is twice the kth natural frequency of the string, supposed fixed at its extremities.

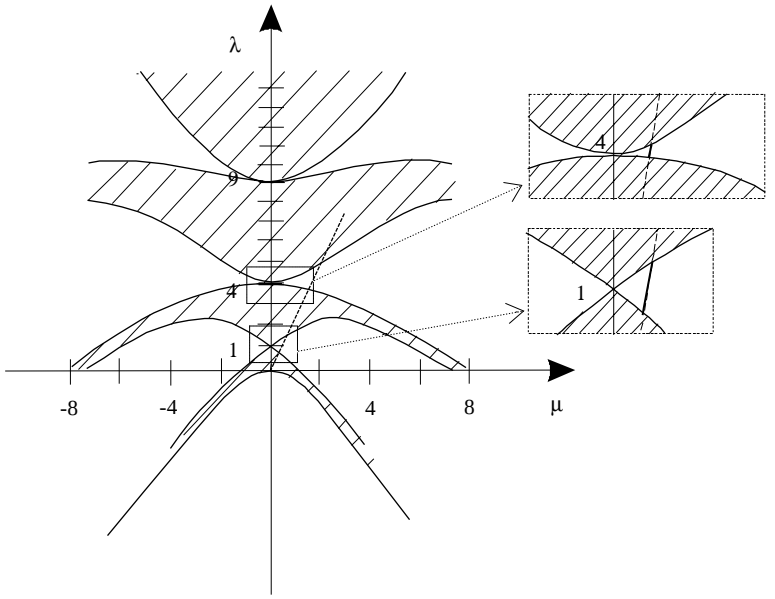

Fig. 3. Stability chart for Mathieu's equation.

Similarly instability occurs when $\lambda_k \simeq 4$, i.e., when the frequency of the pulsing load and the natural frequency of the cable coincide. However, this second condition is to be considered less dangerous than $\lambda_k \simeq 1$, because for the same value of the ratio N_0/P_0, the range of λs for which instability occurs (see Fig. 3) is larger in a neighborhood of $\lambda = 1$ than in a neighborhood of $\lambda = 4$. Recall that, here, the pulsing load $P_0 \sin(2\Omega t)$ models the action transmitted to the stay anchor points by the oscillations of the whole girder which, depending upon traffic or environmental loads, are usually randomly variable in time. Of course, the smaller the resonance interval is, the less is the probability that the frequency Ω remains in that interval for a time sufficiently long to enforce large amplitude oscillations. A similar reasoning can be repeated for the other resonance intervals in neighborhoods of $\lambda = 9, 16$, etc.

In general, environmental or traffic loads may provoke large-amplitude girder oscillations only when in resonance with the overall bridge vibration modes, which implies that 2Ω may be assumed of the same order of the fundamental bridge eigenfrequency. Therefore, the rule of thumb, commonly employed in the design practice, consists in checking that the fundamental eigenfrequency of the bridge is sufficiently distant from twice the fundamental eigenfrequency of each stay, the latter being calculated by supposing the anchorages as fixed points and neglecting the stay bending stiffness and internal damping. Such a criterion is employed in the preliminary design phase also when the principal stays are connected by inter-ties. In this case, it is customary [14] to assume that the net nodes are fixed and consider the free vibrations of the cable portions comprised between two contiguous nodes. This procedure, however, certainly over-estimate the stiffness of the network, considered as a whole and, consequently, the comparison with the fundamental bridge eigenfrequency has to be questioned on theoretical grounds.

3. The continuum model and the auxiliary problem

In order to consider the complex interactions of the various parts of the system (stay, girder and inter-tie), a qualitative approach may be attempted through an equivalent continuum model, obtained by homogenizing the suspension cable network. A "representative-volume-element" $\mathscr{R}$ for such a net is drawn in Fig. 4. The group of fibers drawn horizontally, corresponding to the harp-arranged principal stays of Fig. 1, will be referred to as the *principal* cables, to distinguish them from the *secondary* cables, represented by the two sets of inclined parallel inter-ties.

If the cable net is tight meshed (i.e., formed by numerous small, evenly distributed little cables), one may assume that when it undergoes a small strain accompanied by small rotations, in any region of dimensions comparable with those of $\mathscr{R}$ the strain is homogeneous and the rotation uniform. The corresponding axial force in each of the elements in $\mathscr{R}$ can be easily calculated and, following a well-known procedure sometimes employed in technical applications, one can imagine "smearing" the forces in the fibers onto the boundary of the representative-volume-element $\mathscr{R}$ and consider an equivalent continuous material. Recall from the Introduction that cables have been properly pre-tensioned, so that they can withstand compressive loads as tension decrements. In other words, the net is equivalent to a truss for what its structural response is concerned and, because of its symmetry, the homogenized material results to be an elastic homogeneous and orthotropic membrane, with the orthotropy directions parallel to the vectors $\mathbf{e}_1$ and $\mathbf{e}_2$ of Fig. 4. Assume that cables are made of a linear elastic material, with Young's modulus E, and let their cross sections be equal to A_1 and A_2 for principal and secondary cables, respectively. Using standard notation [20, Chapter 9], the constitutive equations for the equivalent continuum, when referred to a system (x, y) parallel to the axes of orthotropy (Fig. 4), take the form

$$\begin{aligned}
\varepsilon_{xx} &= \frac{1}{E_1}\sigma_{xx} - \frac{\nu_1}{E_1}\sigma_{yy},\\
\varepsilon_{yy} &= -\frac{\nu_2}{E_2}\sigma_{xx} + \frac{1}{E_2}\sigma_{yy},\\
\varepsilon_{xy} &= \frac{1}{2G}\tau_{xy},
\end{aligned} \tag{13}$$

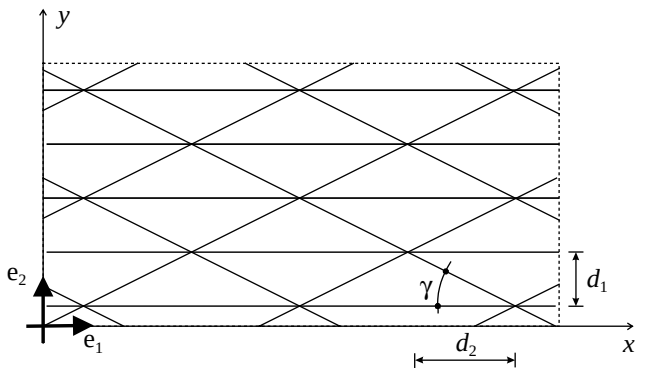

Fig. 4. A representative volume element for the suspension cable net.

where

$$\frac{1}{E_1}=\frac{d_1}{EA_1}h,\quad \frac{1}{E_2}=\left(\frac{d_1}{EA_2\sin^3\gamma\tan\gamma}+\frac{d_1}{EA_1\tan^4\gamma}\right)h,$$
$$\frac{\nu_1}{E_1}=\frac{\nu_2}{E_2}=\frac{d_1}{EA_1\tan^2\gamma}h,\quad \frac{1}{G}=\frac{d_1}{EA_2\cos\gamma\sin^2\gamma}h. \tag{14}$$

Here h is a reference thickness, whereas parameters d_1, γ and $d_2=d_1\cot\gamma$, which define net shape and size, are indicated in Fig. 4.

When the suspension net in Fig. 1 is replaced by homogenized triangle-shaped membranes, an ideal "*web bridge*" is obtained, whose dynamical response may be evaluated analytically. Information about the original network suspended bridge can afterwards be derived through the correspondence established by Eq. (14).

Germane to the dynamical analysis, consider first the static equilibrium of a web bridge subjected to the uniformly distributed load q_0. For, as mentioned in the Introduction, assume that the bridge is of the slender deck type [17]. In the borderline case where the girder has no bending stiffness but is axially rigid and the pylons are stiff, using symmetry considerations, the problem may be simplified as in Fig. 5. Such structure is obtained by connecting a horizontal beam to a wedge-shaped orthotropic elastic membrane, clamped on the vertical side and free on the oblique side. The beam is drawn with many hinges to recall that it is assumed to be perfectly flexible but axially stiff. The elastic problem consists in determining the stress field in the wedge when a vertical, uniformly distributed, load q_0 acts on the beam.

For convenience, introduce the reference system (x,y) and polar co-ordinates (r,θ), such that the orthotropy directions of the wedge-shaped membrane are parallel to axes x and y, corresponding to $\theta=0$ and $\theta=\frac{\pi}{2}$. Let $\{u,v\},\{\sigma_{xx},\sigma_{yy},\tau_{xy}\}$, $\{\varepsilon_{xx},\varepsilon_{yy},\varepsilon_{xy}\}$ represent the displacement, stress and strain components in the (x,y) reference system, while their counterparts in polar co-ordinates will be denoted by $\{u_r,v_\theta\},\{\sigma_{rr},\sigma_{\theta\theta},\tau_{r\theta}\}$ and $\{\varepsilon_{rr},\varepsilon_{\theta\theta},\varepsilon_{r\theta}\}$. In the following, cartesian or polar reference system will be indifferently used whenever more convenient. The

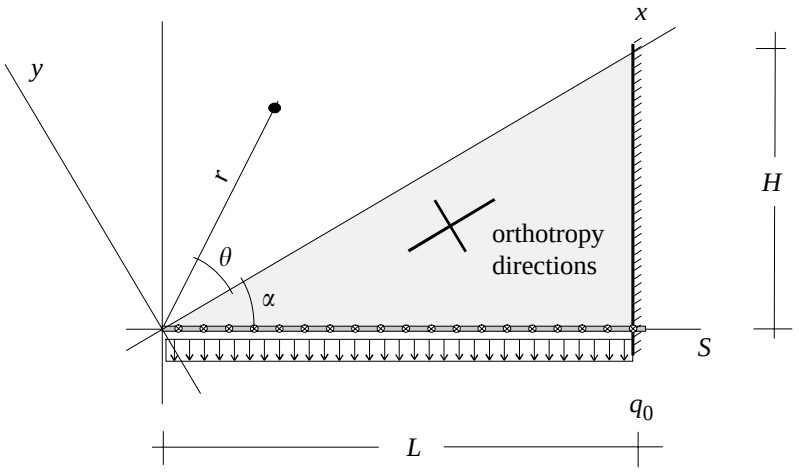

Fig. 5. The auxiliary problem for the wedge-beam assembly.

boundary conditions for this problem take the form

$$\begin{aligned}&\sigma_{\theta\theta} = -q_0/h, \quad \varepsilon_{rr} = 0 \quad \text{for } \theta = -\alpha,\\ &\sigma_{\theta\theta} = 0, \quad \tau_{r\theta} = 0, \quad \text{for } \theta = 0,\\ &u_r = 0, \quad v_\theta = 0 \quad \text{at } r = L/\cos(\theta+\alpha), -\alpha \leqslant \theta \leqslant 0.\end{aligned} \tag{15}$$

Solutions for anisotropic wedges have been discussed, with different approaches, by several authors (see for example Ref. [21], in particular Art. 8.5 of [22], and references therein reported). Despite formalism and solution techniques have been continuously improving [23,24], here reference is made to the original method by Lekhnitskii [20], whose notation presents the great advantage that the material elastic properties can be summarized in just a few parameters (the complex parameters), strictly correlated with the cable-network size and shape.

Following Ref. [20], Art. 5, a plane problem in homogeneous anisotropic elasticity is confined to the selection of a complex stress-function F that verifies the differential equation

$$D_1 D_2 D_3 D_4(F) = 0, \tag{16}$$

where, in polar co-ordinates, the differential operator D_k reads

$$D_k = (\sin\theta - \mu_k \cos\theta)\frac{\partial}{\partial r} + (\cos\theta + \mu_k \sin\theta)\frac{1}{r}\frac{\partial}{\partial\theta}, \quad k = 1, \ldots, 4. \tag{17}$$

Here, μ_k, $k = 1, \ldots, 4$, denotes four complex numbers, in the following referred to as the *complex parameters*. Since they turn out to be the roots of the *characteristic equation*:

$$f(\mu) = \frac{\mu^4}{E_1} + \left(\frac{1}{G} - 2\frac{\nu_1}{E_1}\right)\mu^2 + \frac{1}{E_2} = 0, \tag{18}$$

they synoptically describe the material elastic properties. Once F is known, the stress components in polar co-ordinates are given by

$$\sigma_{rr} = \frac{1}{r}\frac{\partial F}{\partial r} + \frac{1}{r^2}\frac{\partial^2 F}{\partial\theta^2}, \quad \sigma_{\theta\theta} = \frac{\partial^2 F}{\partial r^2}, \quad \tau_{r\theta} = -\frac{\partial^2}{\partial r\,\partial\theta}\left(\frac{F}{r}\right). \tag{19}$$

By considering a stress function of the form

$$F(r,\theta) = r^2 \Phi(\theta), \tag{20}$$

one finds that the boundary conditions $(15)_1$ and $(15)_2$ result from Eq. (19) automatically satisfied. Moreover, the solution that can be obtained from Eq. (20) can be considered sufficiently accurate, provide one accepts an approximation for what condition $(15)_3$ is concerned. Such an approximation is legitimate if the wedge is so long to be considered infinite.

The explicit expression for $\Phi(\theta)$ is found by inserting expression (20) into Eq. (16) and integrating four times successively. As a result,

$$\Phi(\theta) = A\cos(2\theta) + B\sin(2\theta) + C\varphi(\theta) + D, \tag{21}$$

where the constants A, B, C and D are found from the boundary conditions $(15)_1$ and $(15)_2$. In general, the expression for $\varphi(\theta)$ Ref. [20, Art. 7] varies according to the possible nature of the roots of the characteristic equation (18). Two different cases must be distinguished.

In case I, the complex parameters are pure distinct imaginary numbers, say $\mu_1 = \mathrm{i}\beta$, $\mu_2 = \mathrm{i}\delta$, $\mu_3 = \bar{\mu}_1$ and $\mu_4 = \bar{\mu}_2$, with $\beta \neq \delta$. In this situation, after some calculation, one finds that the general

solution for Eq. (16) implies

$$\varphi(\theta) = -\frac{\beta}{\beta^2-\delta^2}(\cos^2\theta - \delta^2\sin^2\theta)\arctan(\delta\tan\theta) + \frac{\delta}{\beta^2-\delta^2}(\cos^2\theta - \beta^2\sin^2\theta)\arctan(\beta\tan\theta) + \frac{\beta\delta}{\beta^2-\delta^2}\sin\theta\cos\theta\ln\frac{\cos^2\theta+\beta^2\sin^2\theta}{\cos^2\theta+\delta^2\sin^2\theta}. \tag{22}$$

In the second case (case II), in which the complex parameters are of the form $\mu_1 = \xi + \mathrm{i}\eta$, $\mu_2 = -\xi + \mathrm{i}\eta$, $\mu_3 = \bar{\mu}_1$ and $\mu_4 = \bar{\mu}_2$, denoting $\mu^2 = \xi^2 + \eta^2$, one finds

$$\begin{aligned}\varphi(\theta) = &-\frac{\xi\eta^2}{\mu^6}\cos(2\theta)\ln\frac{\mu^2\sin^2\theta + 2\xi\sin\theta\cos\theta + \cos^2\theta}{\mu^2\sin^2\theta - 2\xi\sin\theta\cos\theta + \cos^2\theta}\\ &-\frac{4\xi\eta}{\mu^6}\arctan\frac{\eta\cos\theta}{\mu^2\sin\theta + \xi\cos\theta}\\ &\times\left[2\eta^2\cos\theta\left(\sin\theta + \frac{\xi}{\mu^2}\cos\theta\right) + \xi\left(\sin^2\theta + \frac{\xi}{\mu^2}\sin(2\theta) + \frac{\xi^2-\eta^2}{\mu^4}\cos^2\theta\right)\right]\\ &+\frac{4\xi\eta}{\mu^6}\arctan\frac{\eta\cos\theta}{\mu^2\sin\theta - \xi\cos\theta}\\ &\times\left[2\eta^2\cos\theta\left(\sin\theta - \frac{\xi}{\mu^2}\cos\theta\right) - \xi\left(\sin^2\theta - \frac{\xi}{\mu^2}\sin(2\theta) + \frac{\xi^2-\eta^2}{\mu^4}\cos^2\theta\right)\right].\end{aligned} \tag{23}$$

The borderline case when the complex parameters are pure imaginary, but pairwise equal, i.e., $\mu_1 = \mu_2 = \mathrm{i}\beta$, $\mu_3 = \mu_4 = \bar{\mu}_1$, can be obtained by a proper limit of the above expressions. In particular, when the material is isotropic, corresponding to $\mu_1 = \mu_2 = \mathrm{i}$ and $\mu_3 = \mu_4 = -\mathrm{i}$, one easily finds $\varphi(\theta) = \theta$.

For a better characterization of the problem, it is useful to introduce the quantities

$$p = \frac{A_1}{d_1}, \quad q = \frac{A_2}{d_2\sin\gamma} = \frac{A_2}{d_1\cos\gamma}. \tag{24}$$

Their significance is clear from the fact that, denoting with $\mathscr{A} \equiv \frac{1}{2}LH$ the area of the wedge in Fig. 5, the total volume of the material used for the cables is given by $(p+q)\mathscr{A}$, whereas $p\mathscr{A}$ and $q\mathscr{A}$ represent the material quantities used for the principal and secondary cables, respectively. Expressions (14) then become

$$\begin{aligned}&\frac{1}{hE_1} = \frac{1}{pE}, \quad \frac{1}{hE_2} = \frac{1}{Eq\sin^4\gamma} + \frac{1}{Ep\tan^4\gamma},\\ &\frac{\nu_1}{hE_1} = \frac{\nu_2}{hE_2} = \frac{1}{Ep\tan^2\gamma}, \quad \frac{1}{hG} = \frac{1}{Eq\cos^2\gamma\sin^2\gamma}\end{aligned} \tag{25}$$

and the characteristic equation (18) takes the form

$$\frac{\mu^4}{p}+\left(\frac{1}{q\cos^2\gamma\sin^2\gamma}-\frac{2}{p\tan^2\gamma}\right)\mu^2+\frac{1}{q\sin^4\gamma}+\frac{1}{p\tan^4\gamma}=0. \tag{26}$$

In general, it is clear that the principal stays must be much stronger that the secondary cables, since the formers directly sustain the bridge girder, while the latter are usually introduced for a subordinate purpose, (i.e., to inhibit the stay vibrations). Therefore, one may limit consider about the case in which the amount of material used for the principal cables is much greater than that used for the secondary ones, that is $p\gg q$. Under this assumption, Eq. (26) can be simplified by neglecting high order terms in

$$\frac{\mu^4}{p}+\frac{\mu^2}{q\cos^2\gamma\sin^2\gamma}+\frac{1}{q\sin^4\gamma}=0. \tag{27}$$

The discriminant of this equation is positive when $p\gg q$. Consequently, the characteristic parameters, $\mathrm{i}\beta$ and $\mathrm{i}\delta$, are pure imaginary numbers as in case I. Neglecting higher order terms, they take the form

$$\beta\cong\frac{1}{\cos\gamma\sin\gamma}\sqrt{\frac{p}{q}},\quad \delta\cong\frac{1}{\tan\gamma}. \tag{28}$$

It should be noticed that the parameter δ practically depends solely upon the geometry of the network (Fig. 4), whereas β takes into account also the distribution of material between the principal and secondary cables. Indeed, the convenience of Lekhnitskii's notation lies in this direct correlation between the characteristic parameters and the network shape and size.

Determining the constants A, B, C and D appearing in Eq. (21) from conditions $(15)_1$ and $(15)_2$ is not easy, even in case I. A more convenient way to handle the problem is to introduce a complex potential of the generalized complex variables $z_1=x+\mathrm{i}\beta$ and $z_2=x+\mathrm{i}\delta$. Following the generalized complex-variable technique outlined in Ref. [20], the expression of stress, strain and displacement take a concise, convenient form. The corresponding calculations are reported in the appendix for the reader's convenience. The result is that the Cartesian components of the stress field read

$$\begin{aligned}
\sigma_{xx}&=\frac{q_0}{h\sin^2\alpha}\left[1+K_2-\frac{2\beta\delta\sin^2\alpha}{(\beta^2-\delta^2)}K_1\left(\delta\arctan\frac{\delta y}{x}-\beta\arctan\frac{\beta y}{x}\right)\right],\\
\sigma_{yy}&=-\frac{2q_0}{h(\beta^2-\delta^2)}K_1\left(\delta\arctan\frac{\beta y}{x}-\beta\arctan\frac{\delta y}{x}\right),\\
\tau_{xy}&=\frac{q_0\beta\delta}{h(\beta^2-\delta^2)}K_1\ln\frac{x^2+\beta^2y^2}{x^2+\delta^2y^2},
\end{aligned} \tag{29}$$

where K_1 and K_2 are constants. Recalling that $\mathrm{i}\beta$ and $\mathrm{i}\delta$ are the roots of the characteristic equation (18), so that

$$\frac{E_1}{E_2}=\beta^2\delta^2,\quad \frac{E_1}{G}-2\nu_1=\beta^2+\delta^2, \tag{30}$$

the quantities K_1 and K_2 can be written in the form

$$K_1 = (\beta^2 - \delta^2)(\cos^2\alpha - \nu_1 \sin^2\alpha)/\Bigg\{(\beta\delta \sin\alpha\cos\alpha) \times [(\beta^2 + \delta^2)\sin^2\alpha + 2\cos^2\alpha] \ln\left(\frac{1+\beta^2\tan^2\alpha}{1+\delta^2\tan^2\alpha}\right) + 2[\beta \arctan(\delta\tan\alpha) - \delta\arctan(\beta\tan\alpha)][\beta^2\delta^2\sin^4\alpha - \cos^4\alpha]\Bigg\} \tag{31}$$

and

$$K_2 = \frac{2K_1}{\beta^2 - \delta^2}\left\{\delta(\beta^2\sin^2\alpha - \cos^2\alpha)\arctan(\beta\tan\alpha) - \beta(\delta^2\sin^2\alpha - \cos^2\alpha)\arctan(\delta\tan\alpha) - \beta\delta\sin\alpha\cos\alpha\ln\left(\frac{1+\beta^2\tan^2\alpha}{1+\delta^2\tan^2\alpha}\right)\right\}. \tag{32}$$

Having assumed $p \gg q$, one has from (28) that $\beta \gg 1$. Consequently, expanding in Taylor's series (31) and (32), one obtains

$$K_1 = \frac{\cos^2\alpha - \nu_1\sin^2\alpha}{\delta\sin^3\alpha\left[2\delta\sin\alpha\arctan(\delta\tan\alpha) + \cos\alpha\ln\left(\frac{1+\beta^2\tan^2\alpha}{1+\delta^2\tan^2\alpha}\right)\right]} \times \left[\left(\frac{1}{\beta}\right) + 2\delta^2\frac{\sin\alpha\arctan(\beta\tan\alpha)}{2\delta\sin\alpha\arctan(\delta\tan\alpha) + \cos\alpha\ln\left(\frac{1+\beta^2\tan^2\alpha}{1+\delta^2\tan^2\alpha}\right)}\left(\frac{1}{\beta^2}\right) + o\left(\frac{1}{\beta^2}\right)\right] \tag{33}$$

and

$$K_2 = K_1\left[2\delta\sin^2\alpha\arctan(\beta\tan\alpha) + O\left(\frac{1}{\beta}\right)\right]. \tag{34}$$

Notice that both K_1 and K_2 are positive and their order of magnitude is

$$K_1 = O\left(\frac{1}{\beta\ln\beta}\right), \quad K_2 = O\left(\frac{1}{\beta\ln\beta}\right). \tag{35}$$

Consequently, it follows from Eq. (29) that, as expected

$$\sigma_{xx} = \frac{q_0}{h\sin^2\alpha} + o\left(\frac{1}{\beta^2}\right), \quad \sigma_{yy} = o\left(\frac{1}{\beta^2}\right), \quad \tau_{xy} = o\left(\frac{1}{\beta^2}\right). \tag{36}$$

It is easy to verify that in the borderline case when $p/q \to \infty$ and, consequently from Eqs. (25) and (28), $E_2 \to 0$, $G \to 0$, $\nu_1 \to 0$ and $\beta \to +\infty$, the state of stress is given by

$$\sigma_{xx} = \frac{q_0}{h\sin^2\alpha}, \quad \sigma_{yy} = 0, \quad \tau_{xy} = 0. \tag{37}$$

This condition corresponds to the vanishing of the set of secondary stays, i.e., the bridge is a traditional cable-stayed one of the harp type.

For the following considerations, it is necessary to calculate the displacement field. It should be noticed that in a solution of type (20) the two conditions $(15)_1$ and $(15)_2$ are precisely fulfilled, whereas Eq. $(15)_3$ can only approximately be verified. In order to eliminate the indeterminacy of rigid-body motions, one requires instead of Eq. $(15)_3$ that

$$\begin{aligned} &u\cos\alpha - v\sin\alpha = 0 \quad \text{at } (x,y) = (0,0),\\ &u = 0 \quad \text{at } (x,y) = (L\cos\alpha, -L\sin\alpha),\\ &u = 0 \quad \text{at } (x,y) = (L/\cos\alpha, 0). \end{aligned} \tag{38}$$

Calculations can be simplified using the theory of complex potential of generalized complex variable. Referring to the appendix for more details, the displacement expressions for $p/q \gg 1$, and consequently $\beta \gg 1$, take the form

$$\begin{aligned} u(x,y) = \frac{q_0}{E_1 h \sin^2\alpha}\Bigg\{&(1+K_2)\left(x - y\tan\alpha - \frac{L}{\cos\alpha}\right)\\ &+ K_1 y\beta\delta\sin^2\alpha \ln\frac{x^2+\beta^2y^2}{L^2(\cos^2\alpha+\beta^2\sin^2\alpha)}\\ &+2K_1\delta\sin\alpha\left[x\sin\alpha\arctan\frac{\beta y}{x} - y\cos\alpha\arctan(\beta\tan\alpha)\right] + O\left(\frac{1}{\beta^2}\right)\Bigg\}, \end{aligned} \tag{39}$$

$$\begin{aligned} v(x,y) = \frac{q_0}{E_1 h \sin^2\alpha}\Bigg\{&(1+K_2)\left(-v_1 y + x\tan\alpha - \frac{L}{\sin\alpha}\right)\\ &- K_1 x\beta\delta\sin^2\alpha\ln\frac{x^2+\delta^2y^2}{L^2(\cos^2\alpha+\beta^2\sin^2\alpha)} + 2K_1\beta\delta^2 y\sin^2\alpha\arctan\frac{\delta y}{x}\\ &-2K_1\delta\sin\alpha\left[y(\delta^2+v_1)\sin\alpha\arctan\frac{\beta y}{x} - x\cos\alpha\arctan(\beta\tan\alpha)\right] + O\left(\frac{1}{\beta^2}\right)\Bigg\}. \end{aligned} \tag{40}$$

From these formulas, what is important is to calculate the displacement of the horizontal side $y = -x\tan\alpha$ of the wedge, where this is connected to the beam. In particular, the vertical displacement η of the beam is given by

$$\eta = -(u\sin\alpha + v\cos\alpha). \tag{41}$$

For, introducing the co-ordinate s such that (Fig. 5) the horizontal beam has the parametric equation

$$x = s\cos\alpha, \quad y = -s\sin\alpha, \quad 0 \leqslant s \leqslant L, \tag{42}$$

one obtains after simple, though time consuming, calculations

$$\eta = \frac{q_0}{E_1 h\sin^3\alpha}\left[(1+K_2)\frac{L-s}{\cos\alpha} + K_1\beta\delta s\sin^3\alpha\ln\frac{s^2}{L^2} + o\left(\frac{1}{\beta}\right)\right]. \tag{43}$$

To realize how the presence of the secondary stays influence the deflection of the bridge, consider $p/q = 10$ and $\gamma = 45^\circ$, for which $\beta \simeq 6.5$, $\delta \simeq 1$, $K_1 = 0.232$ and $K_2 = 0.086$. This example may be compared through (43) with the borderline case of a classical harp-type cable stayed bridge (with no inter-ties), characterized by $K_1 = 0$ and $K_2 = 0$. The corresponding graphs are juxtaposed in Fig. 6. As expected, since the beam has no bending stiffness, the deformation of

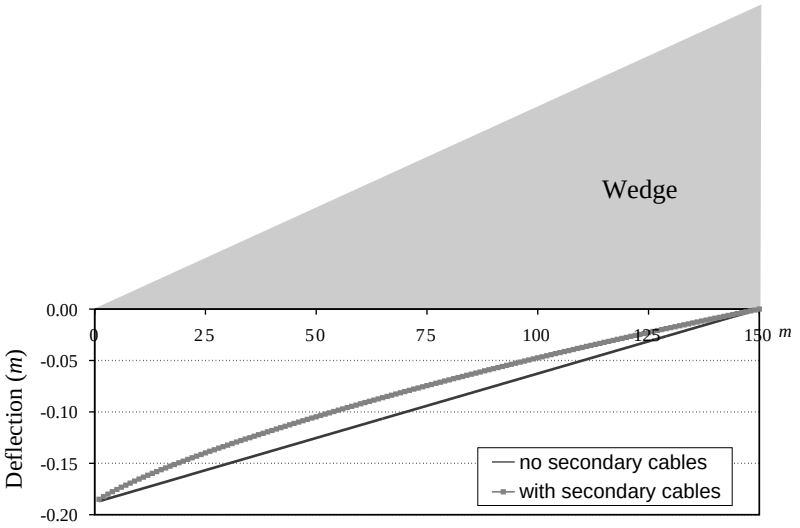

Fig. 6. Girder deflection with and without secondary cables ($L = 150$ m).

the bridge when $K_1 = K_2 = 0$ is a straight line. The deformed shape with secondary cables is always above this line, since any addition of material can only increase the stiffness of the bridge. However, notice that the girder sag close to the bridge mid-span is practically the same in the two conditions, an evident sign that the secondary cables have only a limited influence upon the bridge deflection.

4. The vibrations of the bridge

The influence of the secondary cables upon the vibrations of the whole bridge is now investigated by studying the natural vibrations of the system in Fig. 5. Let ρ represent the mass per unit area of the homogenized orthotropic wedge, and let m be the mass per unit length of the beam connected to the wedge on the horizontal side. Since in any bridge the girder is much heavier than the stays, one may assume $\rho LH/2 \ll mL$. In other words, the overall natural vibrations of the system may be accurately calculated by neglecting the mass of the wedge even if, of course, the influence of ρ will result fundamental when analyzing *local* oscillations (this will be done in the next section).

The fundamental vibration frequency of the system is estimated using Rayleigh's method. The first oscillation mode of the bridge is approximated by its deformed shape due to a load mg, uniformly distributed along the girder. From Eq. (43), neglecting terms of higher order than $1/\beta$, recall that the girder deflection takes the form

$$\bar{\eta}(s) = \frac{mg}{E_1 h \sin^3\alpha}\left[(1+K_2)\frac{L-s}{\cos\alpha} + K_1\beta\delta s \sin^3\alpha \ln\frac{s^2}{L^2}\right], \tag{44}$$

where β, δ, K_1 and K_2 have been defined in Eqs. (28), (31) and (32). The first natural frequency ω of the bridge is consequently estimated by

$$\omega^2 = g\frac{\int_0^L m\bar{\eta}(s)\,\mathrm{d}s}{\int_0^L m\bar{\eta}^2(s)\,\mathrm{d}s} = g\frac{\int_0^L \bar{\eta}(s)\,\mathrm{d}s}{\int_0^L \bar{\eta}^2(s)\,\mathrm{d}s}. \tag{45}$$

Introducing the quantities

$$A = \frac{(1+K_2)}{\cos\alpha}, \quad B = K_1\beta\delta\sin^3\alpha, \tag{46}$$

Eq. (45) becomes

$$\omega^2 = \frac{27}{2}\frac{E_1 h\sin^3\alpha}{mL}\frac{(A-B)}{(9A^2-15AB+8B^2)}. \tag{47}$$

Now, in the borderline case where the secondary cables are absent, since $K_1 = K_2 = 0$, it results in

$$A = \frac{1}{\cos\alpha}, \quad B = 0 \tag{48}$$

and the natural frequency ω_0 reads

$$\omega_0^2 = \frac{3}{2}\frac{E_1 h\sin^3\alpha\cos\alpha}{mL}. \tag{49}$$

In the general case, observing from Eq. (35) that

$$A = \frac{1}{\cos\alpha} + O\left(\frac{1}{\beta\ln\beta}\right), \quad B = O\left(\frac{1}{\ln\beta}\right), \tag{50}$$

and using Eq. (45) one finds that

$$\omega^2 = \omega_0^2\left[1 + O\left(\frac{1}{\ln\beta}\right)\right]. \tag{51}$$

But, recall from Eq. (28) that $\beta \cong (1/\cos\gamma\sin\gamma)\sqrt{p/q}$, where p and q, representative of the material used for principal and secondary stays, respectively, have been defined in Eq. (24). Since the case of interest is when $p/q \gg 1$ and $\beta \gg 1$, from Eq. (51) it is then clear that the set of secondary cables has only a limited influence upon the first natural frequency of the bridge. This finding is not surprising since, as noticed from Fig. 6, the secondary cables do not produce noteworthy modifications of the girder deflection curve.

As an example, consider the following data, taken from a real bridge: $m = 2\times10^4$ kg/m, $L = 135$ m, $\alpha = \arctan(1/2.5)$, $\gamma = 45^\circ$. Moreover, assume that the tensile stress in the principal stays, of Young's modulus $E = 2\times10^{11}$ N/m^2, is $\sigma_0 = 4\times10^8$ N/m^2. When the secondary cables are absent, it results in

$$p = \frac{A_1}{d_1} = \frac{mg}{\sigma_0\sin^2\alpha}, \quad hE_1 = pE \tag{52}$$

and consequently, from Eq. (49), $\omega_0 = 4.335$ rad/s. On the other hand, for $q/p = 0.001$, a reasonable value for a real bridge, one finds from Eq. (28) $\beta = 63.24$, and from Eqs. (31), (32), (46) and (47), $\omega = 4.463$ rad/s, corresponding to an increment of less than 2%.

In conclusion, for the cases of interest ($p/q \gg 1$) the secondary cables have only a limited influence on the first natural vibration mode of the system. Consequently, while estimating the first natural frequency, not a significant error is made if the presence of the secondary cables is neglected. In other words, the network suspension bridge may be considered as an ordinary cable-stayed bridge.

5. The vibrations of the stays

The following analysis, based upon the continuum approach, describes the vibration of the network as a whole, allowing one to evaluate the efficiency of the inter-ties in reducing the natural oscillations of the principal stays.

5.1. The model

Consider the problem represented in Fig. 7. The structural scheme is equal to that in Section 3, with the exception that now the beam is subjected to a uniformly distributed pulsing load $P_1 \sin(2\Omega t)$ in addition to the dead load mg. The cyclic action models the excitation due to traffic or environment, or at least may be thought of to be the first term of a Fourier's expansion. As already mentioned in Section 2, recall that the pulsing part of such actions are usually so feeble that they may induce significant girder oscillations only when in resonance with the overall bridge vibration. This implies that 2Ω is of the same order of the fundamental bridge eigenfrequency, which can be estimated through the analysis of Section 4.

While studying the dynamic equilibrium of the wedge-shaped membrane, its mass-per-unit-area ρ cannot be neglected. Hamilton's principle will be used to derive the equations governing the system vibrations, considering the equilibrium configuration under permanent loads as the reference state. To reach a closed-form solution, a few simplifying hypotheses will be introduced,

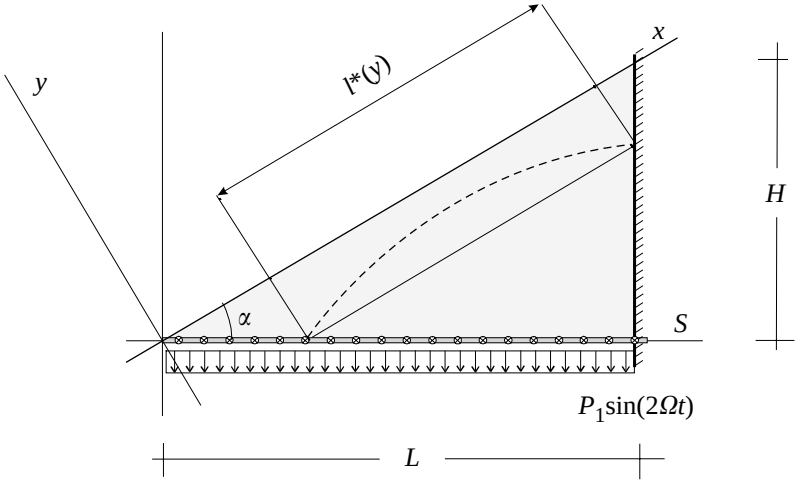

Fig. 7. The wedge-beam model to investigate the parametric resonance phenomenon.

which represent the natural extension to this 2-D case of Kirchhoff hypotheses for the vibrating string, discussed at length in Section 2.

First of all, similarly to Eq. (1), one can surmise that the *incremental* strain of the wedge, measured from the stressed reference state, is given by

$$\varepsilon_{xx} \cong u_{,x} + \frac{v_{,x}^2}{2}, \quad \gamma_{xy} \cong u_{,y} + v_{,x}\,, \quad \varepsilon_{yy} \cong v_{,y}\,, \tag{53}$$

where $u(x,y)$ and $v(x,y)$ represents the *incremental* displacement components in the x and y directions, respectively (Fig. 7). Motivation for this is that the principal cables, parallel to the x-axis, are much stiffer than the secondary ones, so that, since $v_{,x} \gg u_{,x}$, the second order term $v_{,x}^2$ may become comparable with the others. The *incremental* stress components $\{\sigma_{xx}, \sigma_{yy}, \tau_{xy}\}$ are given by

$$\begin{aligned} \sigma_{xx} &= \lambda_{11}\varepsilon_{xx} + \lambda_{12}\varepsilon_{yy}, \\ \sigma_{yy} &= \lambda_{12}\varepsilon_{xx} + \lambda_{22}\varepsilon_{yy}, \\ \tau_{xy} &= \mu\gamma_{xy} \end{aligned} \tag{54}$$

with [20]

$$\lambda_{11} \equiv \frac{E_1}{1-\nu_1\nu_2}, \quad \lambda_{22} \equiv \frac{E_2}{1-\nu_1\nu_2}, \quad \lambda_{12} \equiv \frac{\nu_1 E_2}{1-\nu_1\nu_2}, \quad \mu \equiv G, \tag{55}$$

where E_1, E_2, ν_1, ν_2 and G are related to the cable-net shape and size of Fig. 4 by Eq. (14).

The expression of the potential energy must account for the fact that the system reference configuration is not natural. Denoting with $\{\sigma_{xx}^0, \sigma_{yy}^0, \tau_{xy}^0\}$ the stress state in the membrane under permanent loads, one may assume

$$\sigma_{xx}^0 = \frac{mg}{h\sin^2\alpha}, \quad \sigma_{yy}^0 = 0, \quad \tau_{xy}^0 = 0. \tag{56}$$

These expressions directly follow from Eq. (36) and represent an approximate elastic solution for the system subjected to the dead load mg, uniformly distributed along the beam. Consequently, the potential energy U can be written in the form [25, Section 2.5]

$$\begin{aligned} U = {} & h\int_{\mathscr{B}} \sigma_{xx}^0\varepsilon_{xx}\,\mathrm{d}x\,\mathrm{d}y + \frac{1}{2}h\int_{\mathscr{B}} (\lambda_{11}\varepsilon_{xx}^2 + \lambda_{22}\varepsilon_{yy}^2 + \mu\gamma_{xy}^2)\,\mathrm{d}x\,\mathrm{d}y \\ & + \int_{\Gamma} mg[\sin\alpha\, u(s\cos\alpha, -s\sin\alpha) + \cos\alpha\, v(s\cos\alpha, -s\sin\alpha)]\,\mathrm{d}s, \end{aligned} \tag{57}$$

where $\mathscr{B}$ denotes reference domain of the wedge, Γ is its horizontal boundary (where the wedge is connected to the beam) and the co-ordinate s is defined in Fig. 7. Similarly to Section 2, where the weight of the string was neglected with respect to the weight of the suspended mass M (Fig. 2), the term

$$h\int_{\Omega} \rho g(u\sin\alpha + v\cos\alpha)\,\mathrm{d}x\,\mathrm{d}y$$

has not been considered in Eq. (57).

Moreover, since the stiffness of the principal stays refrains motions in the x direction, we expect that $v_{,t} \gg u_{,t}$. The kinetic energy T is thus approximated by

$$T = \frac{h\rho}{2} \int_{\Omega} (v_{,t}(x,y))^2 \, \mathrm{d}x \, \mathrm{d}y + \frac{m}{2} \int_{\Gamma} [(u_{,t}(s \sin\alpha, -s\cos\alpha))^2 + (v_{,t}(s\sin\alpha, -s\cos\alpha))^2] \, \mathrm{d}s. \tag{58}$$

Finally, the work done by the uniformly distributed pulsing load $P_1 \sin(\Omega t)$ reads

$$W = -\int_{\Gamma} P_1 \sin(2\Omega t)(u(s\sin\alpha, -s\cos\alpha)\sin\alpha + v(s\sin\alpha, -s\cos\alpha)\cos\alpha) \, \mathrm{d}s. \tag{59}$$

Using expressions (57)–(59) in Hamilton's principle

$$\delta(T - U) = \delta W, \tag{60}$$

the final result is the system of differential equations

$$\sigma_{xx,x} + \tau_{xy,y} = 0, \tag{61}$$

$$\tau_{xy,x} + \sigma_{yy,y} + \frac{mg}{h\sin^2\alpha} v_{,xx} + \frac{\partial}{\partial x}(\sigma_{xx} v_{,x}) - \rho v_{,tt} = 0 \tag{62}$$

with boundary conditions

$$\begin{aligned} &\text{at } y = 0, && \sigma_{yy} = 0, \quad \tau_{xy} = 0, \\ &\text{at } y = x\cot\alpha - L/\sin\alpha, && u = 0, \quad v = 0, \\ &\text{at } y = -x\tan\alpha, && \begin{cases} u\cos\alpha - v\sin\alpha = 0, \\ -mw_{,tt} - P_1 \sin(2\Omega t) + h(\sigma^0_{xx} v_{,x} \sin\alpha\cos\alpha + \sigma_{nn}) = 0. \end{cases} \end{aligned} \tag{63}$$

For simplicity's sake, in Eq. $(63)_3$, the beam displacement component in vertical direction is denoted by $w = -(u\sin\alpha + v\cos\alpha)$, while σ_{nn} $(= \sigma_{xx}\sin^2\alpha - 2\tau_{xy}\sin\alpha\cos\alpha + \sigma_{yy}\cos^2\alpha)$ represents the normal component of stress in the membrane on the line $y = -x\tan\alpha$.

What should be noticed is that the non-linear effects in Eq. (62) are due to the term $\frac{\partial}{\partial x}(\sigma_{xx} v_{,x})$. A simplified though accurate analysis can be obtained if, here, one considers for σ_{xx} the stress corresponding to the static solution for the distributed load $P_1 \sin(2\Omega t)$. Recall that this hypothesis is similar to that commonly accepted for the vibrating string: in Section 2 the *incremental* axial force in the string coincided with the static solution for a straight cable under the action of the pulsing load $P_0 \sin(2\Omega t)$ (see Fig. 2). Referring to the analysis of Section 3, using Eq. (36) one may write

$$\frac{\partial}{\partial x}(\sigma_{xx} v_{,x}) \cong \frac{P_1 \sin(2\Omega t)}{h\sin^2\alpha} v_{,xx}. \tag{64}$$

Consequently, Eqs. (61) and (62) reduce to the *linear* system of differential equations

$$\sigma_{xx,x} + \tau_{xy,y} = 0, \tag{65}$$

$$\tau_{xy,x} + \sigma_{yy,y} + \frac{mg + P_1 \sin(2\Omega t)}{h\sin^2\alpha} v_{,xx} - \rho v_{,tt} = 0. \tag{66}$$

Regarding the boundary conditions, referring again to the simplifications used in the 1-D case, instead of Eq. $(63)_{3-4}$, the alternative conditions

$$\left.\begin{array}{l} u=0 \\ v=0 \end{array}\right\} \quad \text{at } y=-x\tan\alpha, \tag{67}$$

having a strict analogy with Eq. $(3)_{2-3}$, where the end points of the string were considered to be fixed and the axial load variable in time. Here, the end points of fibers $y = const$ are constrained but, nevertheless, possible variations in the stress σ_{xx} are included through the pulsing term $P_1 \sin(2\Omega t)$ appearing in Eq. (66). It is the presence of such a term that may give rise to the possibility of parametric resonance.

In summary, the problem is governed by the system of differential equations (65) and (66), with boundary conditions $(63)_1$, $(63)_2$ and (67). From this equations, adding proper initial conditions, the system motion is determined.

5.2. Qualitative solutions

Before addressing the general problem, it is useful to consider first a few borderline cases.

5.2.1. Absence of secondary cables

The simplest case is when the secondary cables are absent. Letting $A_2 \to 0$ in Eq. (14), one obtains from Eq. (55)

$$\lambda_{11} \simeq E_1, \quad \lambda_{12} \simeq 0, \quad \lambda_{22} \simeq 0, \quad v_1 \simeq 0, \quad |v_2| < \infty.$$

System (65), (66), taking into account Eqs. (54), (55) and expressions (53) for ε_{xx}, ε_{yy} and γ_{xy}, reduces to

$$\frac{\partial}{\partial x}\left(u_{,x} + \tfrac{1}{2} v_{,x}^2\right) = 0,$$

$$\frac{mg + P_1 \sin(2\Omega t)}{\sin^2\alpha} - \rho h v_{,tt} = 0. \tag{68}$$

No partial derivatives with respect to y appear in these expression, so that one can consider the problem separately on the lines $y = const$. In fact, it is clear that when the secondary cables are vanishing, every fiber disposed parallel to the x axes can move independently from the surrounding ones. In other words, it is as if the wedge was made of independent, parallel wires.

The one-dimensional solution of Section 2 is thus easily recovered. Following the method of separation of variables, consider

$$v(x, y, t) = \Psi(x, y)\Phi(y, t), \tag{69}$$

which, after substitution in Eq. $(68)_2$, gives

$$\frac{mg + P_1 \sin(2\Omega t)}{\sin^2\alpha} \frac{\Psi_{,xx}}{\Psi} - \rho h \frac{\Phi_{,tt}}{\Phi} = 0$$

and the following eigenvalue problem

$$\frac{\Psi_{,xx}}{\Psi} + \zeta(y) = 0, \tag{70}$$

$$\Phi_{,tt} + \frac{mg + P_1 \sin(2\Omega t)}{\rho h \sin^2\alpha}\zeta(y)\Phi = 0 \tag{71}$$

for some unknown function $\zeta = \zeta(y)$. From Eq. (70), the general expression for Ψ is

$$\Psi(x,y) = A(y)\sin(x\sqrt{\zeta(y)}) + B(y)\cos(x\sqrt{\zeta(y)}) \tag{72}$$

and the boundary conditions $(63)_2$ are automatically satisfied. In order to respect Eq. (67), $A(y)$ and $B(y)$ in Eq. (72) must satisfy the system

$$A(y)\sin\left[\left(\frac{L}{\cos\alpha} + y\tan\alpha\right)\sqrt{\zeta(y)}\right] + B(y)\cos\left[\left(\frac{L}{\cos\alpha} + y\tan\alpha\right)\sqrt{\zeta(y)}\right] = 0,$$
$$A(y)\sin\left[-y\cot\alpha\sqrt{\zeta(y)}\right] + B(y)\cos\left[-y\cot\alpha\sqrt{\zeta(y)}\right] = 0.$$

Requiring that the determinant of this system is zero, one obtains

$$\sin\left[\left(\frac{L}{\cos\alpha} + \frac{y}{\sin\alpha\cos\alpha}\right)\sqrt{\zeta(y)}\right] = 0,$$

which gives

$$\sqrt{\zeta(y)} = \frac{k\pi}{((L/\cos\alpha) + (y/\sin\alpha\cos\alpha))} = \frac{k\pi}{l^*(y)}, \tag{73}$$

where k is an integer number and

$$l^*(y) \equiv \frac{L}{\cos\alpha} + \frac{y}{\sin\alpha\cos\alpha},$$

evidenced in Fig. 7, represents the length of fibers parallel to the x-axis at y. Consequently $\Psi(x,y)$ now reads

$$\Psi(x,y) = A(y)\sin\left[\frac{k\pi}{l^*(y)}\left(\frac{L}{\cos\alpha} + y\tan\alpha - x\right)\right],$$

where $A(y)$ represents the (undetermined) amplitude of the oscillations of the fiber at y. The analogy with the vibrating string problem is immediate.

The displacement component $u(x,y,t)$ can be found a posteriori from Eq. $(68)_1$. Supposing it is of the form

$$u(x,y,t) = \Xi(x,y)\,\Phi(y,t), \tag{74}$$

where $\Phi(y,t)$ is the same as in Eq. (69), one finds that $\Xi(x,y)$ is the solution of the differential equation

$$\Xi_{,xx} = -\frac{1}{2}\frac{\partial}{\partial x}(\Psi_{,x})^2,$$

with boundary conditions $(63)_2$ and (67).

Observe that by posing $P_1 = 0$ in Eq. (71), recalling Eq. (73), one obtains that fibers at position $y = const$ vibrate with a cyclic frequency given by

$$\omega_0^2 = \frac{mg}{h\rho \sin^2\alpha}\left(\frac{k\pi}{l^*(y)}\right)^2. \tag{75}$$

This represents the natural fiber frequency. The correspondence with Eq. (9) is easily seen.

The stability of the fibers at $y = const$ is then governed by the Mathieu's equation (71) which, because of Eq. (73), becomes

$$\Phi_{,tt} + \frac{mg + P_1 \sin(2\Omega t)}{h\rho \sin^2\alpha}\left(\frac{k\pi}{l^*(y)}\right)^2 \Phi = 0. \tag{76}$$

The corresponding discussion is analogous to that presented for the unidimensional problem in Section 2 through the stability chart of Fig. 3. In particular, the cyclic frequency 2Ω of the pulsing load has to be compared with ω_0 defined in Eq. (75).

5.2.2. Secondary cables slightly inclined to the main stays

As a second case, suppose that the angle γ that the secondary cables forms with the principal ones is very small, i.e., $\gamma \to 0$. From Eq. (14), the order of magnitude of the elastic moduli is

$$E_2 = E_1 O(\gamma^8), \quad \frac{1}{\nu_1} = O(\gamma^4), \quad \nu_2 = O(\gamma^8), \quad G = E_1 O(\gamma^4) \tag{77}$$

and consequently, from Eq. (55)

$$\lambda_{11} = O(E_1), \quad \lambda_{22} = \lambda_{11} O(\gamma^8), \quad \lambda_{12} = \lambda_{11} O(\gamma^4), \quad \mu = \lambda_{11} O(\gamma^4). \tag{78}$$

Thus, recalling (53) and (54), neglecting higher order terms, expression (65) reduces to

$$\frac{\partial}{\partial x}\left(u_{,x} + \frac{v_{,x}^2}{2}\right) = 0. \tag{79}$$

Concerning Eq. (66), one observes that since γ is assumed very small, one may anticipate that $\varepsilon_{xx} \ll \varepsilon_{yy}$. Consequently, because of Eq. (78), the stress component σ_{yy} results to be very small. For the same reasons, it is natural to expect $u_{,yx} \ll v_{,xx}$. Consequently, keeping only the leading terms in Eq. (66), the following equation is obtained:

$$\left(\frac{mg + \mu h \sin^2\alpha + P_1 \sin(2\Omega t)}{\rho h \sin^2\alpha}\right) v_{,xx} - v_{,tt} = 0. \tag{80}$$

It is immediate to recognize that Eqs. (79) and (80) are perfectly analogous to Eqs. $(68)_1$ and $(68)_2$, provided one substitutes the quantity mg with $(mg + \mu h \sin^2\alpha)$. Moreover, observe that no partial derivative with respect to the y variable is present in Eqs. (79) and (80), so that $v(x, y, t)$ can still be though of as written in the form (69). Repeating the same analysis of Section 5.2.1, one

obtains a condition analogous to Eq. (73). A posteriori, in proximity of the free edge, Eq. $(63)_1$ can still be considered identically satisfied up to higher order terms.

Therefore, in this case the stability condition can be discussed by examining equation

$$\Phi_{,tt}+\frac{mg+\mu h\sin^2\alpha+P_1\sin(2\Omega t)}{\rho h\sin^2\alpha}\left(\frac{k\pi}{l^*}\right)^2\Phi=0, \tag{81}$$

which takes the place of Eq. (76).

The fact that any fiber parallel to the x-axis can be thought of as vibrating independently from the neighboring ones, is a consequence of the assumption $\gamma\ll 1$. If γ is very small (Fig. 4), the resistance that the secondary cables offers to the mutual approaching of any two consecutive principal stays is consequently reduced (recall that from Eq. (77) one has $E_2=O(\gamma^8)$). Moreover, by comparing Eqs. (76) and (81), it follows that *the effect of the secondary cables is equivalent to an apparent tensile-stress increase* in the principal stays, percentage-wise equal to

$$i_{\%}=\frac{\mu h\sin^2\alpha+mg}{mg}. \tag{82}$$

This effect is in favor of the stability of the system.

5.2.3. Secondary cables orthogonal to the main stays

A third important case is when $\gamma=\frac{1}{2}\pi$. Now, since $d_1=d_2\tan\gamma$, it follows from (14)

$$E_1h=\frac{EA_1}{d_1},\quad E_2h=\frac{EA_2}{d_2},\quad v_1=v_2=0,\quad G=0, \tag{83}$$

so that, using Eq. (55),

$$\lambda_{11}=E_1,\quad \lambda_{22}=E_2,\quad \lambda_{12}=\mu=0.$$

Again, it is logical to expect $u_{,xy}\ll v_{,xx}$. Neglecting higher order terms, the governing system of differential equations reads

$$\frac{\partial}{\partial x}\left(u_{,x}+\frac{v_{,x}^2}{2}\right)=0, \tag{84}$$

$$\lambda_{22}hv_{,yy}+\frac{mg+P_1\sin(2\Omega t)}{\sin^2\alpha}v_{,xx}-\rho hv_{,tt}=0 \tag{85}$$

with boundary conditions $(63)_{1-2}$ and (67). In particular, the second of Eq. $(63)_1$ is automatically satisfied, whereas $\sigma_{yy}=0$ implies $v_{,y}=0$ at $y=0$.

What should be noticed in Eq. (85) is the term $\lambda_{22}hv_{,yy}$ which, on the contrary to the preceding cases, establishes that the fibers at $y=const$ cannot vibrate independently one another. The secondary cables should thus give a strong contribution in enhancing the stability of the system.

The analytic discussion of system (84) and (85) is not immediate. One may tentatively investigate solutions of the type

$$v(x,y,t)=\Lambda(x,y)\Phi(t).$$

Table 1
Parameters C_1 and C_2 for different values of the wedge angle α

Cot α	1	1.5	2	2.5	3	3.5
C_1	10.00	13.63	15.45	16.45	17.04	17.44
C_2	10.00	13.55	37.03	61.24	91.54	127.71

Multiplying Eq. (85) by Λ and integrating other the domain Ω, and noticing that because of the boundary conditions the identities

$$\int_{\mathscr{B}} \frac{\partial}{\partial x}(\Lambda_{,x}\,\Lambda)\,\mathrm{d}a = \int_{\partial\mathscr{B}} (\Lambda_{,x}\,\Lambda) n_x\,\mathrm{d}l = 0,$$

$$\int_{\mathscr{B}} \frac{\partial}{\partial y}(\Lambda_{,y}\,\Lambda)\,\mathrm{d}a = \int_{\partial\mathscr{B}} (\Lambda_{,x}\,\Lambda) n_y\,\mathrm{d}l = 0$$

hold, one obtains

$$\left(\lambda_{22} h \int_{\mathscr{B}} (\Lambda_{,y})^2\,\mathrm{d}a + \frac{mg + P_1 \sin(2\Omega t)}{\sin^2\alpha} \int_{\mathscr{B}} (\Lambda_{,x})^2\,\mathrm{d}a\right)\Phi + \rho h \ddot{\Phi} \int_{\mathscr{B}} \Lambda^2\,\mathrm{d}a = 0. \tag{86}$$

Following Rayleigh's method, $\Lambda(x,y)$ may be selected in the form

$$\Lambda(x,y) = \tfrac{1}{4}(-y^2 + x^2\tan^2\alpha)\left[-y^2 + \left(\frac{L}{\sin\alpha} - \frac{x}{\tan\alpha}\right)^2\right]. \tag{87}$$

The evaluation of the integrals that appear in Eq. (86) presents no difficulty and can be easily performed either analytically or numerically. Table 1 gives C_1 and C_2 as functions of the angle α of the wedge, where

$$C_1 = L^2 \frac{\int_{\mathscr{B}} (\Lambda_{,x})^2\,\mathrm{d}a}{\int_{\mathscr{B}} \Lambda^2\,\mathrm{d}a}, \quad C_2 = L^2 \frac{\int_{\mathscr{B}} (\Lambda_{,y})^2\,\mathrm{d}a}{\int_{\mathscr{B}} \Lambda^2\,\mathrm{d}a}. \tag{88}$$

The system vibration is thus governed by Mathieu's equation

$$\left(\lambda_{22} h \frac{C_2}{L^2} + \frac{mg + P_1 \sin(2\Omega t)}{\sin^2\alpha} \frac{C_1}{L^2}\right)\Phi + \rho h \ddot{\Phi} = 0. \tag{89}$$

The natural vibration frequency ω_0 of the cable net, considered as a whole, may be obtained by posing $P_1 = 0$ in Eq. (89), to give

$$\omega_0^2 = \frac{1}{\rho h L^2}\left(\lambda_{22} h C_2 + \frac{mg C_1}{\sin^2\alpha}\right). \tag{90}$$

This value can be compared with that given by Eq. (75) in Section 5.2.1, corresponding to the absence of secondary cables. For, recalling that parameters q and p of Eq. (24) indicate the quantity of material employed for the principal and secondary cables respectively, from Eqs. (55) and (14) it follows, as an order of magnitude

$$E_2 h = \lambda_{22} h = qE, \quad mg \simeq \sigma_{adm} \frac{A_1}{d_1} = \sigma_{adm} p, \tag{91}$$

where σ_{adm} represents the design stress in the principal stays. Thus, from Eq. (91),

$$\frac{\lambda_{22}h}{mg} = O\left(\frac{q}{p}\frac{\sigma_{adm}}{E}\right).$$

Observing that for steel cables $E/\sigma_{adm} = O(10^3)$, the great efficiency of the secondary cables in enhancing the natural vibration frequencies of the stays is clear.

The stability analysis from Mathieu's equation (89) is straightforward. Introducing $\tau = \Omega t$, the canonical form

$$\frac{\mathrm{d}^2\Phi}{\mathrm{d}\tau^2} + \left[\left(\frac{\lambda_{22}C_2}{\rho\Omega^2L^2} + \frac{mg\,C_1}{h\rho\sin^2\alpha\Omega^2L^2}\right) + \frac{P_1C_1}{h\rho\sin^2\alpha\Omega^2L^2}\sin(2\tau)\right]\Phi = 0 \tag{92}$$

is obtained. Recalling Eq. (90), this expression can also be written in the form

$$\frac{\mathrm{d}^2\Phi}{\mathrm{d}\tau^2} + \left[\left(\frac{\omega_0}{\Omega}\right)^2 + 2\left(\left(\frac{\omega_0}{\Omega}\right)^2\frac{P_1}{N}\right)\sin(2\tau)\right]\Phi = 0,$$

where N is a characteristic parameter, having the dimension of a length, equal to

$$N = \frac{2\omega_0^2h\rho L^2\sin^2\alpha}{C_1} = \frac{2}{C_1}(\lambda_{22}hC_2\sin^2\alpha + mgC_1).$$

The corresponding discussion is analogous to that of the unidimensional case and can again be done referring to the stability chart in Fig. 3. Also in this case, it is important to check that the cyclic frequency 2Ω is sufficiently far away from twice the natural frequency ω_0.

5.2.4. Approximate solution for the general case

The analytical study of the system of equations (65) and (66) in the most general case is so difficult that in general a numerical approach should be envisaged. An engineering approach, that has proved to be satisfactory in some practical case, is to give an approximate solution consisting in a combination of the two limit cases analyzed in Sections 5.2.2 and 5.2.3. Despite that all the elastic moduli are now different from zero, one may imagine that, according to the analysis of Section 5.2.2, the presence of the μ modulus is equivalent to an apparent increase in the stress acting in the principal stays according to Eq. (82). In practice, one sets $\mu = 0$, but conventionally increase the permanent load mg to the ratio r defined as

$$r = \frac{\mu h\sin^2\alpha + mg}{mg}.$$

It follows that the resulting system of differential equations is analogous to that considered in Section 5.2.3. Repeating the same analysis, considering again a shape function $\Lambda(x, y)$ of the form (87), the natural cyclic frequency of the cable net is given by an expression analogous to Eq. (90), but where mg is substituted by rmg. The discussion of the stability of the system follows the same rationale leading to Eq. (92).

6. Example and discussion

To illustrate the practical use of the continuum approach in one example, the method is now applied to the layout of the Normandy Bridge. Recently, built in France [14–16], with its 856 m main span the structure represents one of the grandest cable-stayed bridges in the world. Due to its daring size, a particular attention had to be paid to the stay design since, apart from technological problems, their length constituted the bridge vulnerable point. To mention just one aspect, 55% of the transverse bridge *gabarit* is formed by the stay sheaths: only considering he wind pressure, one can imagine the order of magnitude of the transverse forces transmitted to the stays. The risk of parametric-resonance-induced cable vibrations had been evidenced from the beginning, by comparing the natural frequencies of the whole structure, obtained by modelling the cables as truss members, and the natural frequencies of the stays, calculated supposing them fixed at their anchorage points.

For medium-span bridges, the cable vibrations may be reduced by dampers but, on the Normandy Bridge scale, the efficiency of such a countermeasure is limited and the only practicable solution is a system of secondary inter-ties. These were preliminarily designed by considering the nodes fixed and calculating the axial force in the resulting cable portions due to wind action, modelled as a static pressure of $3\ \mathrm{kN/m^2}$ [14]. This preliminary study, later corroborated by more refined numerical analysis [14], suggested the use of only four secondary cables for each stay plane, according to the scheme of Fig. 8. Of course, the secondary cables have no effect if the stays vibrate at right angle to the plane in which they are contained, but practical experience has shown that this vibration mode is much less frequent than in-plane oscillations. This is probably due to the stay initial sag under its own weight, which causes the stay to straighten and start moving in the vertical plane, when the anchorage points are displaced apart.

Many different layouts were considered for the secondary cables. At first, pseudo-curvilinear profiles, similar to Leonhardt's design for crossing the Messina strait [13], were proposed. Later, this solution was disregarded due to the difficulties in regulating the cable tension in the construction phase. The rectilinear disposal of Fig. 8, with secondary cables almost at right angle to the principal stays, was definitely selected. A precise program was followed to progressively tension the secondary cables to avoid their slackening, and a particular sheathing was conceived to increase the intrinsic cable damping [14].

It is now discussed whether the assumptions of the continuum approach of Section 5.1 do apply to this structure. The Normandy bridge is of the slender deck type, since the girder height, for aerodynamic reasons, is contained in only 3 m (1/285 of the bridge main span). Thus, at least as a first order approximation, the girder flexural inertia, as well as its axial deformation, can be neglected. On the other hand, the pylons constitute quite a rigid constraint, since they are anchored by robust back stays to side spans, which are further stiffened by intermediate piers at a fair distance one from the other (see Fig. 8).

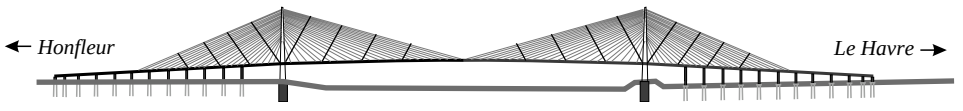

Fig. 8. Layout of the Normandy Bridge (France, 1994).

As far as the stays are concerned, they were pre-tensioned to avoid slackening under live loads. However, neither the cross section of the principal stays is constant, nor the stays follow the harp pattern (the layout is of the semi-harp type). Notice, however, that the longest stays are sensibly parallel one another and their cross-section almost constant. Now, the bridge deflection, as well as its dynamical response, is governed by the elasticity of the stays anchored in proximity of the mid-span, while the short stays play a side role, since they connect the girder where it already rests on pylons. Therefore, when considering the homogenized web-bridge, one may tentatively pretend that the layout determined by the longest stays is ideally prosecuted throughout the bridge. In other words, the original layout is approximated by a harp-type layout, where cables are parallel to the longest stays and maintain the same cross-section.

Under these hypotheses, it is possible to correlate the real bridge with the auxiliary problem of Fig. 5. The following data are taken from Refs. [14,15]. Let $2L = 856$ m represent the length of the bridge main span, $H = 161$ m be the height of the pylons above the girder and $\alpha = \arctan(H/L) = 20.6^\circ$ be the angle formed by the longest stays with the horizontal. Let $i = 19.65$ m denote the relative distance between stay anchor points to the girder, $m = 6.5$ t/m the mass per unit length of half of the girder (i.e., that portion supported by each one of the two stay planes of the bridge) and $L_s \cong L/\cos\alpha = 457$ m the length of the longest principal stay. Let $A_1 = 74.20$ cm^2 be their cross-sectional area (they are composed of 56 steel 0.6″-tendons) and $m_s = 8000 \times 74.2 \times 10^{-4} = 59.36$ kg/m the corresponding mass per unit length. Consider then a triangle-shaped cable net as in Fig. 4, for which $d_1 = i\sin\alpha = 6.92$ m represents the interaxial distance between principal stays.

Neglecting the girder flexural stiffness, the axial load in the principal stays is approximately

$$\sigma_s = \frac{mgi}{A_1 \sin\alpha} = 47.94 \text{ kN/cm}^2.$$

Thus, from the analysis of Sections 2 and 5.2.1, the circular frequency corresponding to the first natural vibration mode for the longest stay results

$$\omega_s = \frac{\pi}{L_s}\sqrt{\frac{\sigma_s A_1}{m_s}} = 1.68 \text{ rad/s} \tag{93}$$

and the corresponding period $T_s = 3.75$ s.

In order to evaluate the natural frequencies of the whole bridge, we refer to Section 4. When no secondary cables are present, formula (49) applies, to give

$$\omega_0 = \sqrt{\tfrac{3}{4}\sin 2\alpha \frac{Eg}{\sigma_s L}} = 2.10 \text{ rad/s}, \quad T_0 = 2.9 \text{ s}. \tag{94}$$

When, in general, secondary cables are added, Eq. (47) should be used instead, but when $p/q \gg 1$ (the only case of interest), since the complex parameter β becomes very large (recall Eqs. (24) and (28)), the approximation furnished by Eq. (49) is satisfactory. In other words, the value in Eq. (94) does not vary sensibly when a moderate warp of secondary cables is added.

The effect of inter-ties upon the vibration of the cable net is established using the results of Section 5. First consider the layout of the real bridge, sketched in Fig. 8. From Ref. [14], the following data have to be considered for the net (see Fig. 4): $A_2 = 2.80$ cm^2 as the cross-sectional

area of each secondary cable; $\gamma = \pi/2$ as the angle formed by the secondary cables with the principal ones; $d_2 = 57.1$ m as the interaxial distance of the secondary cables.

Recalling Eqs. (24), (25) and (55), it is easily found

$$\lambda_{11}h = E_1 h = \frac{EA_1}{d_1} = 2144 \text{ kN/cm}, \quad \lambda_{12}h \cong 0,$$

$$\lambda_{22}h = E_2 h = \frac{EA_2}{d_2} = 9.8 \text{ kN/cm}, \quad \mu h \cong 0,$$

where h is the reference thickness of the equivalent continuous wedge-shaped membrane. Moreover, from Eq. (24),

$$p = \frac{A_1}{d_1} = 0.1072 \text{ cm}^2/\text{cm}, \quad q = \frac{A_2}{d_2 \sin\gamma} = 4.9 \times 10^{-4} \text{ cm}^2/\text{cm}, \quad \frac{p}{q} = 219.$$

Thus, the assumed estimation $p/q \gg 1$, which justified the asymptotic expansions for $\beta \to \infty$ and $\delta \to 0$, is very well verified in this case.

Now, the wedge density ρ is given by

$$\rho h \cong 8000\,(p+q) = 8.62 \text{ kg/m}^2.$$

Since $H/L = 161/428$, using Eq. (88) the values $C_1 = 16.67$ and $C_2 = 70.15$ are calculated. The natural cyclic frequency can thus be estimated, from Eq. (90), as

$$\omega^2 = \frac{1}{\rho L^2}\left(\lambda_{22}C_2 + \frac{mgC_1}{h\sin^2\alpha}\right) = 43.58 + 5.42 = 49.00 \text{ rad/s}^2,$$
$$\omega = 7.0 \text{ rad/s}, \tag{95}$$

to which corresponds the natural period $T = 0.9$ s. What should be noticed, in any case, is the great efficiency of the secondary cables in enhancing the natural frequency. Recall that in absence of any connection, the frequency of the longest stay is, from (93), $\omega_s = 1.68$ rad/s ($T_0 = 2.9$ s).

To investigate further, consider an alternative layout where secondary cables, while maintaining the same interaxial distance, are each formed by one 0.6″ tendon at an angle $\gamma = \pi/36$ ($\sim 5^\circ$) with respect to the principal stays. From Eq. (24) it is found that

$$p = \frac{A_1}{d_1} = 0.1072 \text{ cm}^2/\text{cm}, \quad q = \frac{A_2}{d_2 \sin\gamma} = 2.03 \times 10^{-3} \text{ cm}^2/\text{cm}, \quad \frac{p}{q} = 53,$$

and from Eqs. (25) and (55)

$$\lambda_{11}h = 2184 \text{ kN/cm}, \quad \lambda_{12}h = 0.306 \text{ kN/cm},$$

$$\lambda_{22}h = 0.00234 \text{ kN/cm}, \quad \mu h = 0.306 \text{ kN/cm}.$$

Recall, from the analysis developed Section 5.2.2, that when γ is very small the vibrations of the principal stays are practical independent one from the other. Using Eq. (82), the first natural cyclic frequency of the longest stays reads

$$\omega_s = \frac{\pi}{L_s}\sqrt{\frac{mg + \mu h \sin^2\alpha}{\rho h \sin^2\alpha}} = 1.73 \text{ rad/s}. \tag{96}$$

Comparing this value with $\omega_s = 1.68$ rad/s ($T_s = 2.9$ s) in Eq. (93), with no inter-ties, it immediately follows that the obtainable benefit is very small, i.e., *arrangements with γ small are not very efficient*.

As a third possibility, imagine now that secondary cables are placed at an angle $\gamma = \pi/4$, still maintaining fixed $d_2 = 57.1$ m. In this case

$$p = 0.1072 \text{ cm}^2/\text{cm}, \quad q = 6.93 \times 10^{-4} \text{ cm}^2/\text{cm}, \quad p/q = 155, \quad \rho = 8.63 \text{ kg/m}^2,$$

$$E_1 h = 2144.5 \text{ kN/cm}, \quad E_2 h = 3.421 \text{ kN/cm}, \quad \nu_1 = 1, \quad \nu_2 = 0.0016$$

$$\lambda_{11} h = 2148 \text{ kN/cm}, \quad \lambda_{12} h = 3.427 \text{ kN/cm}, \quad \lambda_{22} h = 3.427 \text{ kN/cm}, \quad \mu h = 3.465 \text{ kN/cm}.$$

Using the results of Section 5.2.4, the first natural cyclic frequency of the stay plane is equal to

$$\omega^2 = \frac{1}{\rho L^2}\left(\lambda_{22} C_2 + \frac{(mg + \mu h \sin^2\alpha) C_1}{h \sin^2\alpha}\right) = 15.20 + 5.41 + 3.65 = 24.6 \text{ rad/s}^2, \tag{97}$$

corresponding to $\omega = 4.95$ rad/s and $T = 1.27$ s. Comparing this value with Eq. (95), one notices that this disposal is better than the previous one, but the layout actually used for the Normandy Bridge ($\gamma \cong \pi/2$) is still stiffer.

As a final example, the case with $d_2 = 57.1$ m and $\gamma = \pi/3$ is analyzed for which:

$$p = 0.1072 \text{ cm}^2/\text{cm}, \quad q = 5.66 \times 10^{-4} \text{ cm}^2/\text{cm}, \quad p/q = 189.3, \quad \rho = 8.62 \text{ kg/m}^2,$$

$$E_1 h = 2144.5 \text{ kN/cm}, \quad E_2 h = 6.340 \text{ kN/cm}, \quad \nu_1 = 0.333, \quad \nu_2 = 9.85 \times 10^{-4}$$

$$\lambda_{11} h = 2145 \text{ kN/cm}, \quad \lambda_{12} h = 2.120 \text{ kN/cm}, \quad \lambda_{22} h = 6.342 \text{ kN/cm}, \quad \mu h = 2.120 \text{ kN/cm}.$$

Still referring to Section 5.2.4, the cyclic frequency is now given by

$$\omega^2 = \frac{1}{\rho L^2}\left(\lambda_{22} C_2 + \frac{(mg + \mu h \sin^2\alpha) C_1}{h \sin^2\alpha}\right) = 28.16 + 5.42 + 2.24 = 35.82 \text{ rad/s}^2, \tag{98}$$

corresponding to $\omega = 5.98$ and $T = 1.04$ s. This value is intermediate between those obtained for $\gamma = \pi/4$ and $\pi/2$.

The synthetic approach, which allows for a synoptic comparison of different configurations of the secondary cables, can be of help in designing optimal cable stay arrangements. In particular, this study seems to confirm that when the angle that secondary cables form with the principal stays is small ($\gamma \cong 0$), the efficiency of the connection is limited. The principal stays may vibrate practically independently from one another, and the effect of the secondary warp is only equivalent to a virtual (small) increment of their normal tensile force, as stated by Eq. (82). The stays' natural frequencies are enhanced most when the secondary cables are placed almost at right angle to the principal stays ($\gamma \cong \pi/2$). For intermediate values of γ, the efficiency of the secondary cables can be estimated to be between these two borderline cases, increasing in general with increasing γ.

Checking against the risk of parametric-resonance-induced cable vibrations consists in verifying that the principal eigenfrequency of the whole bridge, given by Eq. (94), is sufficiently distant from twice the fundamental eigenfrequency of the stay. In this respect, the efficiency of different

configurations of secondary stays may be immediately evaluated by comparing Eq. (94) with Eqs. (93), (95)–(96), (97) or (98).

In conclusion, the simple and concise formulas obtained from the continuum approach allow a ready determination of the order of magnitude of the characteristic parameters governing the dynamic response of the bridge. In particular, it is possible to take into account the interaction between contiguous stays when connected by secondary cables and to conceive optimal layouts to enhance the overall natural frequencies of the network. Concerning the latter point, the conclusions are in agreement with the cable arrangement adopted for the Normandy Bridge, for which an orthogonal mesh was selected.

Appendix

The solution of a plane problem in anisotropic linear elasticity theory can be obtained using a generalization of Gousart's complex representation method. Referring to Ref. [20, Chapter II] for a résumé of the technique, here just a few results are recalled. When the complex parameters, solutions of the characteristic equation (18), are pure distinct imaginary numbers, say $\mu_1 = \mathrm{i}\beta$, $\mu_2 = \mathrm{i}\delta$, $\mu_3 = \bar{\mu}_1$ and $\mu_4 = \bar{\mu}_2$ (case I of Section 3), the generalized complex numbers

$$z_1 \equiv x + \mathrm{i}\beta y, \quad z_1 \equiv x + \mathrm{i}\delta y \tag{A.1}$$

are defined. Then, it can be verified that the complex potential $F(x, y)$, introduced in Eq. (16), can be expressed as the real part of the complex function $\hat{F}(z_1, z_2)$, i.e.,

$$F(x, y) = 2\mathrm{Re}[\hat{F}(z_1, z_2)]. \tag{A.2}$$

For example, for the case of Section 3, one can directly verify that F, previously expressed in polar co-ordinates by Eqs. (20) and (21), assumes the simple form

$$\begin{aligned} F(x, y) &= 2\mathrm{Re}[\hat{F}(z_1, z_2)] \\ &= 2\mathrm{Re}\left[\hat{A}\frac{\beta^2 z_2^2 - \delta^2 z_1^2}{2(\beta^2 - \delta^2)} + \hat{B}i\frac{\beta z_2^2 + \delta z_1^2}{4\beta\delta} + \hat{C}\hat{\varphi}(z_1, z_2) + \hat{D}\frac{z_2^2 - z_1^2}{2(\beta^2 - \delta^2)}\right], \end{aligned} \tag{A.3}$$

where

$$\hat{\varphi}(z_1, z_2) = \frac{1}{2(\beta^2 - \delta^2)}(\beta z_2^2 \ln z_2 - \delta z_1^2 \ln z_1). \tag{A.4}$$

Here, the principal representation of the logarithm where the anomaly is comprised in the interval $(-\pi, \pi)$ has been selected.

The theory of generalized complex variables [20] furnishes the expression of the stress components

$$\sigma_{xx} = 2\mathrm{Re}\left[(\mathrm{i}\beta)^2\frac{\partial^2\hat{F}}{\partial z_1^2} + (\mathrm{i}\delta)^2\frac{\partial^2\hat{F}}{\partial z_2^2}\right],$$

$$\sigma_{yy} = 2\mathrm{Re}\left[\frac{\partial^2\hat{F}}{\partial z_1^2} + \frac{\partial^2\hat{F}}{\partial z_2^2}\right],$$

$$\tau_{xy} = -2\mathrm{Re}\left[\mathrm{i}\beta\frac{\partial^2\hat{F}}{\partial z_1^2} + \mathrm{i}\delta\frac{\partial^2\hat{F}}{\partial z_2^2}\right] \tag{A.5}$$

and the displacement field

$$u = 2\mathrm{Re}\left[a_1\frac{\partial\hat{F}}{\partial z_1} + a_2\frac{\partial\hat{F}}{\partial z_2}\right] - \omega y + u_0,$$

$$v = 2\mathrm{Re}\left[b_1\frac{\partial\hat{F}}{\partial z_1} + b_2\frac{\partial\hat{F}}{\partial z_2}\right] + \omega x + v_0 \tag{A.6}$$

with

$$a_1 = \frac{1}{E_1}(\mathrm{i}\beta)^2 - \frac{\nu_1}{E_1}, \quad a_2 = \frac{1}{E_1}(\mathrm{i}\delta)^2 - \frac{\nu_1}{E_1},$$

$$b_1 = -\frac{\nu_1}{E_1}(\mathrm{i}\beta) + \frac{1}{E_2(\mathrm{i}\beta)}, \quad b_2 = -\frac{\nu_1}{E_1}(\mathrm{i}\delta) + \frac{1}{E_2(\mathrm{i}\delta)}. \tag{A.7}$$

On the free edge of equation $y = 0$ (see Fig. 5), from Eqs. $(A.5)_2$ and $(A.5)_3$ the boundary conditions read

$$\mathrm{Re}\left[\frac{\partial\hat{F}}{\partial z_1} + \frac{\partial\hat{F}}{\partial z_2}\right]_{z_1=x,\, z_2=x} = 0, \tag{A.8}$$

$$\mathrm{Re}\left[\mathrm{i}\beta\frac{\partial\hat{F}}{\partial z_1} + \mathrm{i}\delta\frac{\partial\hat{F}}{\partial z_2}\right]_{z_1=x,\, z_2=x} = 0, \tag{A.9}$$

from which $\hat{A} = 0$ and $\hat{B} = 0$ in (A.3). Moreover, conditions $(15)_1$ become

$$\sigma_{xx}\left(\frac{\cos^2\alpha}{E_1} - \frac{\nu_1}{E_1}\sin^2\alpha\right) + \sigma_{yy}\left(\frac{\sin^2\alpha}{E_2} - \frac{\nu_1}{E_1}\cos^2\alpha\right) - \frac{\tau_{xy}}{G}\sin\alpha\cos\alpha = 0,$$

$$\sigma_{xx}\sin^2\alpha + \sigma_{yy}\cos^2\alpha - 2\tau_{xy}\sin\alpha\cos\alpha = \frac{q_0}{h},$$

which, taking into account Eq. (A.5), give

$$\hat{C} = -\frac{q_0}{h}K_1, \quad \hat{D} = \frac{q_0(1+K_2)}{2h\sin^2\alpha} \tag{A.10}$$

with K_1 and K_2 defined in Eqs. (31) and (32).

The displacement components can be calculated from Eq. (A.6), and give expressions (39) and (40).

References

[1] A.M. Abdel-Ghaffar, M.A. Khalifa, Importance of cable vibration in dynamic of cable-stayed bridges, Journal of Engineering Mechanics, American Society of Civil Engineers 117 (1990) 2571–2589.

[2] J. Mathivat, J. Brault, Le pont de Brotonne, Travaux 492 (2) (1976) 22–43.

[3] S.F. Stiemer, P. Taylor, D.H. Vincent, Full scale dynamic testing of the Annacis Bridge, IABSE Periodica 1 (1988) 1–16.
[4] H.E. Langsoe, O.D. Larsen, Generating mechanisms for cable stay oscillations at the Faro Bridges, in: Proceedings of the International Conference on Cable Stayed Bridges, Bangkok, 1987, pp. 1023–1033.
[5] S.V. Ohlsson, Dynamic characterization of cable-stayed bridge—nonlinearities and weakly coupled modes of vibration, in: Proceedings of the International Conference on Cable Stayed Bridges, Bangkok, 1987, pp. 421–431.
[6] D. Murià-Vila, R. Gomèz, C. King, Dynamic structural properties of cable-stayed Tampico Bridge, Journal of Structural Engineering, American Society of Civil Engineers 117 (1991) 3396–3413.
[7] K.A. Jakobsen, E. Jordet, S.K. Rambjor, A.A. Jakobsen, Full scale measurements of the behavior of the Helgeland bridge, a cable stayed bridge located in a harsh environment, in: Proceedings of the International Symposium on Cable Dynamics, Liège, 1995, pp. 473–480.
[8] J.M. Cremer, C. Cournasse, V.V. Goyet, A. Lothaire, A. Dumortier, The stays, their dynamic behavior, their equipments—bridges at Ben–Ahin, Wandre and upon Alzette, in: Proceedings of the International Symposium on Cable Dynamics, Liège, 1995, pp. 489–496.
[9] Y. Hikami, N. Shiraishi, Rain-wind induced vibrations of cables in cable stayed bridges, Journal of Wind Engineering and Industrial Aerodynamics 29 (1988) 409–418.
[10] I. Kovàcs, Zur Frage der Seilschwingungen und der Seildämpfung, Die Bautechnik 59 (1982) 325–332.
[11] J.L. Lilien, A. Pinto da Costa, Vibration amplitudes caused by parametric excitation of cable stayed structures, Journal of Sound and Vibration 174 (1994) 69–90.
[12] E. Caetano, A. Cuhna, C.A. Taylor, Investigation of dynamic cable–deck interaction in a physical model of a cable stayed bridge, part I: modal analysis, Earthquake Engineering Structural Dynamics 29 (2000) 481–498.
[13] F. Leonhardt, W. Zellner, Comparative investigation between suspension bridges and cable-stayed bridges for spans exceeding 600 meters, IABSE-Publications 32 (1972) 127–165.
[14] M. Virlogeux, Les études du pont de Normandie, Travaux 686 (4) (1993) 10–27.
[15] M. Virlogeux, Normandie Bridge—design and construction, Proceedings Institution Civil Engineers—Structures and Buildings 99 (1993) 281–302.
[16] M. Virlogeux, Recent evolution of cable stayed bridges, Engineering Structures 21 (1999) 737–755.
[17] R. Walther, B. Houriet, W. Isler, P. Moia, Cable Stayed Brides, Thomas Telford, London, 1988.
[18] R. Rothe, I. Szabò, Höhere Mathematik, Teubner Verlagsgesellschaft, Stuttgart, 1953.
[19] G. Kirchhoff, Mechanik, Teubner, Lipsia, 1883.
[20] S.G. Lekhnitskii, Anisotropic Plates, Gordon and Breach, New York, 1968.
[21] T.C.T. Ting, Solutions for the anisotropic elastic wedge at critical wedge angles, Journal of Elasticity 24 (1990) 1–20.
[22] T.C.T. Ting, Anisotropic Elasticity, Oxford University Press, New York, 1996.
[23] T.C.T. Ting, A modified Lekhnitskii formalism a la Stroh for anisotropic elasticity and classifications of the 6×6 matrix N, Proceedings Royal Society of London A 455 (1999) 69–89.
[24] T.C.T. Ting, Recent developments in anisotropic elasticity, International Journal of Solids and Structures 37 (2000) 401–409.
[25] M. Biot, Mechanics of Incremental Deformation, Wiley, New York, 1965.